Negative refraction in time-varying, strongly-coupled plasmonic antenna-ENZ systems: Supplementary Information

V. Bruno[1,†], C. DeVault[2,3,†], S. Vezzoli[4,†], Z. Kudyshev[2,3], T. Huq[4], S. Mignuzzi[4], A. Jacassi[4], S. Saha[2,3], Y.D. Shah[1], S.A. Maier[4,7], D.R.S. Cumming[6], A. Boltasseva[2,3], M. Ferrera[5], M. Clerici[6], D. Faccio[1,*], R. Sapienza[4,*], V.M. Shalaev[2,3,*]

[1] *School of Physics and Astronomy, University of Glasgow, G12 8QQ Glasgow, United Kingdom*

[2] *Purdue Quantum Science and Engineering Institute, Purdue University 1205 West State Street, West Lafayette, Indiana 47907, USA*

[3] *School of Electrical and Computer Engineering and Birck Nanotechnology Center, Purdue University, 1205 West State Street, West Lafayette, Indiana 47907, USA*

[4] *The Blackett Laboratory, Department of Physics, Imperial College London, London SW7 2BW, United Kingdom*

[5] *Institute of Photonics and Quantum Sciences, Heriot-Watt University, EH14 4AS Edinburgh, United Kingdom*

[6] *School of Engineering, University of Glasgow, G12 8LT Glasgow, United Kingdom and*

[7] *Chair in Hybrid Nanosystems, Nanoinstitute Munich, Faculty of Physics, Ludwig-Maxilimians-Universitat Munchen, 80539 Munchen, Germany**

I. METASURFACE FABRICATION

Our metasurface is based on a 500×500 μm 2D pattern of gold nano-antenna deposited on top of 40 nm thickness of ITO on a glass substrate. A bi-layer of poly methyl methacrylate (PMMA) was spin coated on top of the ITO film and then baked (first layer 40min, second layer overnight at 180 °C). The designs were patterned onto the resist using a Vistec VB6 electron beam lithography tool. A 5/30 nm layer of Ti/Au was deposited using a Plassys electron beam evaporator. After lift-off, the sample was then cleaned in acetone and isopropyl alcohol. The 40 nm thick ITO layer was purchased by Präzisions Glas & Optik.

II. ENZ MODES OF ITO FILMS

A thin ENZ layer supports surface modes close to the plasma frequency called an ENZ mode [1, 2]. To find the dispersion of the ENZ mode of our bare ITO films, we solve the following dispersion equation for modes of a three layer structure

$$f(\beta,\omega) = 1 + \frac{\epsilon_1\gamma_3}{\epsilon_3\gamma_1} - i\tan(\kappa d)\left(\frac{\epsilon_2\gamma_3}{\epsilon_3\kappa} + \frac{\epsilon_1\kappa}{\epsilon_2\gamma_1}\right) = 0. \quad (1)$$

In Eq. 1, ω is the angular frequency, β is the transverse wavenumber, $k_o^2 = \omega^2/c^2$ is the free space wavenumber, $\gamma_{1,3} = \pm\sqrt{\epsilon_{1,3}k_o^2 - \beta^2}$ are the longitudinal wavenumber in the superstrate ($i = 1$) and superstrate ($i = 3$), and $\kappa = \sqrt{\beta^2 - \epsilon_2 k_o^2}$ is the longitudinal wavenumber in the ITO layer. Here, we choose to solve Eq. 1 using a real β, complex ω approach in order to capture the transient radiative decay behavior of the ENZ mode. Fig. 1 shows solutions of Eq. 1 (i.e. dispersion curves) for both long (blue lines) and short (red line) range surface plasmon modes of the ITO thin films. It is evident that the long range mode is an ENZ mode since the dispersion is nearly flat for a large range of transverse wavevectors β near the screened plasma frequency (i.e. the frequency at which ϵ is close to zero). Because the long range surface modes for a 40nm ITO film occur at frequencies less than the screened plasma frequency, we expect the resonance splitting will be red-shifted from the exact ENZ wavelength.

III. COUPLED HARMONIC OSCILLATOR MODEL

In Figure 2 we show the simulated transmission spectra for Au antennas sitting on top of a bare glass substrate (left panel) and on a 40 nm thick ITO layer (right panel). The black dashed lines describe the behaviour expected

* daniele.faccio@glasgow.ac.uk, r.sapienza@imperial.ac.uk, shalaev@purdue.edu: †These authors contributed equally.

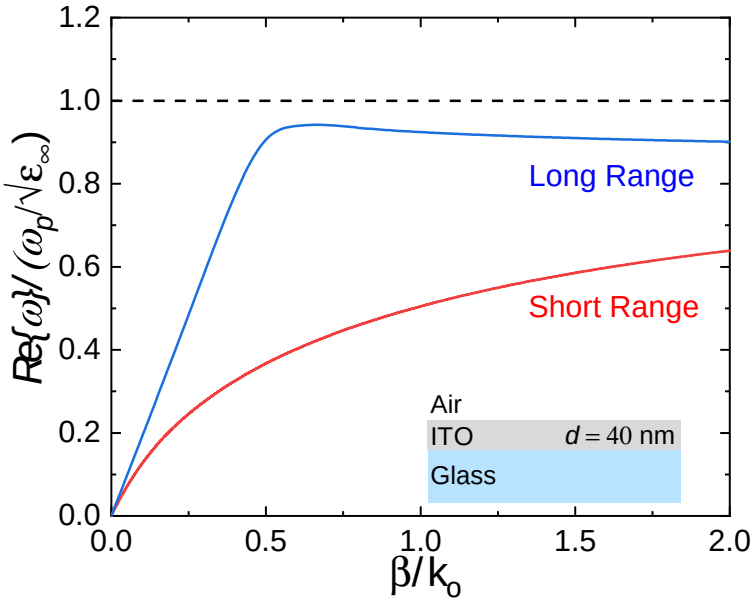

Figure 1. Dispersion relation of the air-ENZ-glass three-layered system (see inset) for 40 nm ITO film. The long (short) range plasmon is indicated with a blue(red) line. The long range plasmon approaches the screened plasma frequency (i.e. ENZ wavelength) for large wavevectors β, as indicated by the nearly flat dispersion.

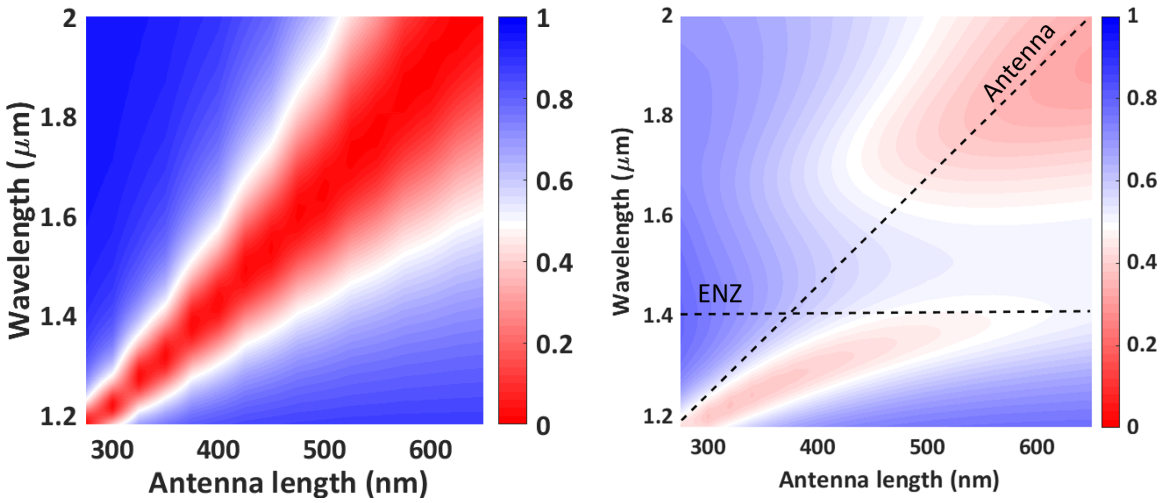

Figure 2. FDTD simulation of transmission spectra for Au antenna on a glass substrate (Left panel) and Au antennas on a 40 nm ITO film (right panel). The horizontal and oblique black dashed lines represent the λ_{ENZ} and the resonance of the Au antennas on a glass substrate, respectively.

in absence of strong coupling. For an antenna sitting on a bare glass substrate, the transmission spectra exhibits a dip due to the dipole-like plasmonic resonance of the antenna. When the Au antenna and the ENZ layer are brought together, the metal resonance is split into two polariton branches near the crossing point of the non-coupled case. As we move away from the strong coupling regime we can see that the resonance of the antenna is slightly red-shifted with respect to the isolated case (left panel). This can be explained by the fact that the ITO layer exhibits an index of refraction $n < 1$ for wavelengths larger than λ_{ENZ}, which causes a redshift of the plasmonic resonance. It was shown in [3–5] that in the limit of thick ENZ layer, i.e. ENZ substrate, this resonance is also expected to be "pinned" at the λ_{ENZ} due the strong dispersion in the ENZ region.

We use a coupled harmonic oscillator model to retrieve the Rabi splitting of strong coupling system based on gold nanoantenna on top of deeply sub-wavelength ITO film. First, consider two coupled harmonic oscillators and write the system of equation for the harmonic mode amplitude of oscillator one $x_1(\omega)$ and two $x_2(\omega)$ as,

$$\begin{pmatrix} \omega_1 - \omega - i\gamma_1 & g \\ g & \omega_2 - \omega - i\gamma_2 \end{pmatrix} \begin{pmatrix} x_1(\omega) \\ x_2(\omega) \end{pmatrix} = i \begin{pmatrix} f_1(\omega) \\ f_2(\omega) \end{pmatrix} \tag{2}$$

where ω is the frequency, $\omega_{1,2}$ and $\gamma_{1,2}$ are the resonance frequency and damping rates of oscillator one and two, respectively, $f_{1,2}(\omega)$ are the harmonic driving forces on oscillator one and two, respectively, and g is the coupling constant between the two oscillators. The eigenvalues of the system are solved by setting the determinant of the 2x2 matrix to zero and solving the resulting quadratic equation. The two complex eigenvalues are then given by,

$$\omega_{\pm} = \frac{1}{2}\left[\omega_1 + \omega_2 - i(\gamma_1 + \gamma_2)\right] \pm \frac{1}{2}\sqrt{(\omega_1 - \omega_2 - i(\gamma_1 - \gamma_2))^2 + 4g^2}. \tag{3}$$

The real portion of $\omega_{\pm}$ gives the dispersion of the eigenvalues, while the imaginary portion dictates the line width [6]. To retrieve the coupling constant of our sample, we fit the experimental resonance minimas to the real portion of Eq. 3. Figure 3 shows the fits (solid lines) to the experimental transmission data points (circles), along with a horizontal line indicating the ENZ wavelength of the film. We extract a coupling constant of $g = 112.1$ meV, corresponding to a Rabi slitting ($\hbar\Omega_R = 2g$) of $\hbar\Omega_R = 224.2$ meV for a 40 nm ITO sample.

To verify our system is in the strong coupling regime, we compare the Rabi frequency to the average dissipation, $\langle\gamma\rangle = (\gamma_1 + \gamma_2)/2$, of the antenna ($\gamma_1$) and the ENZ films ($\gamma_2$). We calculate the dissipation term for the antenna by fitting a Lorentzian function to the bare antenna transmission spectrum (i.e. antenna on a glass substrate) that is resonant at the crossing frequency to extract the linewidth ($\gamma_1 = 197.4$ meV). For the ENZ film dissipation term, we use the imaginary frequency solution to the dispersion relation (Supp. Eq. 1) at large wavevectors ($\gamma_2 = 33.98$ meV). We find an average dissipation of $\langle\gamma\rangle = 115.7$ meV. Indeed, in our system, $\hbar\Omega_R > \langle\gamma\rangle$ which quantitatively shows we are in the strong coupling regime. We can define the Rabi efficiency as $\Delta\omega/\omega_{ENZ}$, where $\Delta\omega$ is the spectral separation of the two transmission deeps and ω_{ENZ} is the frequency where the ϵ crosses zero. At zero detuning between the two resonances ($\lambda_{ant} - \lambda_{ENZ}$), the Rabi level splitting is $\sim 30\%$ of the ENZ frequency [7].

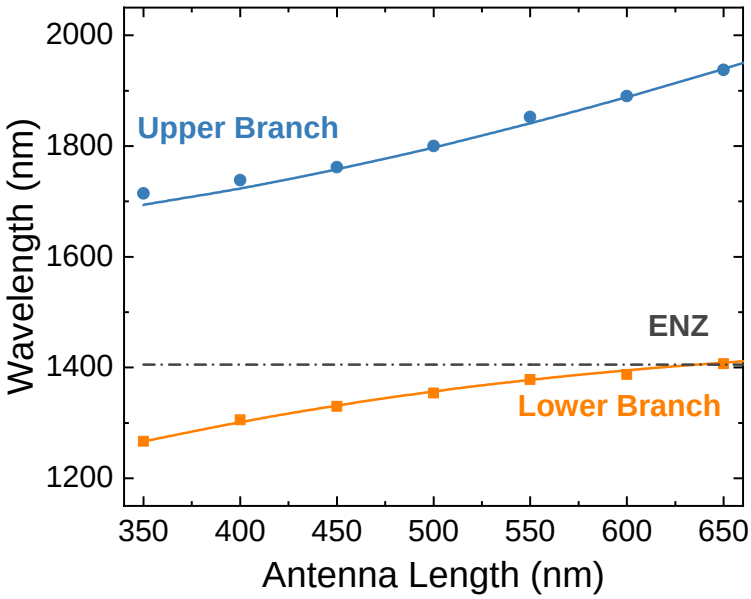

Figure 3. Wavelengths of the transmission minimum as a function of antenna length. Blue (Red) dots: minimum experimental transmission of ENZ (antenna) mode . Blue (Red) line: theoretical fit of the coupled harmonic oscillator model to the ENZ (antenna) mode. Black horizontal dashed (dashed dot) line: ENZ wavelength of the bare ITO film.

IV. MODEL FOR THE FWM INTERACITON

The nonlinear generation of beams in a FWM process can be modelled from the distribution of linear fields, as described for instance by [8]. In this section we will sketch the derivation of Eq. 1 of the main text used to model the FWM process in the strongly coupled system. The nonlinear polarization density $\mathbf{P}(\mathbf{r},\omega)$ for the FWM process leading to the emission of a negative refraction (NR) or phase conjugate (PC) beam can be written as:

$$\mathbf{P}(\mathbf{r},\omega) = \epsilon_0 \boldsymbol{\chi}^{(3)}(\omega) \vdots \mathbf{E}_p^2(\mathbf{r},\omega)\mathbf{E}_s^*(\mathbf{r},\omega) \tag{4}$$

where the $\vdots$ indicate a triple scalar tensor product between $\chi^{(3)}$ and the three fields interacting in the nonlinear medium. The nonlinear polarization current density inside the medium

$$\mathbf{j}(\mathbf{r},\omega) = -i\omega\mathbf{P}(\mathbf{r},\omega)$$

is the source for the non-linear NR (or PC) field $\mathbf{E}$ at the position of the detector, in the far-field. Such field can be estimated by means of the reciprocity theorem. The reciprocity theorem states that a source (a current density) and a detector (a field), in two distinct volumes, can be interchanged such that

$$\int_{V_1} \mathbf{j}_1 \cdot \mathbf{E}_2 \; dV = \int_{V_2} \mathbf{j}_2 \cdot \mathbf{E}_1 \; dV$$

with $\mathbf{j}_1$, $\mathbf{E}_1$, $\mathbf{j}_2$, $\mathbf{E}_2$ are the current densities and the fields in the volumes V_1 and V_2 respectively. In our case we have:

$$\int_{V_{det}} \mathbf{j}_{det} \cdot \mathbf{E} \; dV = \int_{V_{ITO}} \mathbf{j} \cdot \mathbf{E}_{det} \; dV \tag{5}$$

where we introduced a dummy current density $\mathbf{j}_{det}$ in the volume V_{det} at the position of the detector, which produces a (linear) field $\mathbf{E}_{det}$ in the volume of the ITO, V_{ITO}. A dipole current $\mathbf{j}_{det}$ in the far-field generates a plane wave travelling in the direction of NR (or PC). $\mathbf{j}_{det}$ is a point source (prop. to $\delta(\mathbf{r})$) oscillating in the direction of the generated field E and we consider only the component of the electric field E parallel to the direction of the antennas:

$$j_{det}E = \int_{V_{ITO}} \mathbf{j} \cdot \mathbf{E}_{det} \; dV$$

By combining this with Eq. 4 we obtain the final formula of the main text:

$$E(\omega) \propto \int_{V_{ITO}} \mathbf{P}(\mathbf{r},\omega) \cdot \mathbf{E}_{det}(\mathbf{r},\omega) dV. \tag{6}$$

Or by writing explicitly all the fields:

$$E(\omega) \propto \int_{V_{ITO}} \epsilon_0 \boldsymbol{\chi}^{(3)}(\omega) \vdots \mathbf{E}_p^2(\mathbf{r},\omega)\mathbf{E}_s^*(\mathbf{r},\omega) \cdot \mathbf{E}_{det}(\mathbf{r},\omega) dV \tag{7}$$

The efficiency of the FWM process is proportional to the intensity of the NR field $|E|^2$. It is convenient to evaluate the ratio of the efficiency in the strongly coupled metasurface of ITO with gold antennas compared to that of bare ITO, so that the unknown spectral dependence of $\boldsymbol{\chi}^{(3)}(\omega)$ factors out:

$$\eta_{norm}(\omega) = |E_{metasurface}|^2 / |E_{ITO}|^2 \tag{8}$$

Moreover by taking the ratio one can also rule out any experimental contribution to the spectral dependence, for instance due to slightly different pump intensity or collection efficiency at different wavelengths, as any variation will affect equally the NR efficiency spectra with or without antennas.

All fields in Eq. 7 are calculated numerically by FDTD with plane wave illumination using Lumerical.

[1] S. Vassant, A. Archambault, F. Marquier, F. Pardo, U. Gennser, A. Cavanna, J.-L. Pelouard, and J.-J. Greffet, Physical review letters **109**, 237401 (2012).

[2] S. Vassant, J.-P. Hugonin, F. Marquier, and J.-J. Greffet, Opt. Express **20**, 23971 (2012).
[3] J. Kim, A. Dutta, G. V. Naik, A. J. Giles, F. J. Bezares, C. T. Ellis, J. G. Tischler, A. M. Mahmoud, H. Caglayan, O. J. Glembocki, *et al.*, Optica **3**, 339 (2016).
[4] C. T. DeVault, V. A. Zenin, A. Pors, K. Chaudhuri, J. Kim, A. Boltasseva, V. M. Shalaev, and S. I. Bozhevolnyi, Optica **5**, 1557 (2018).
[5] T. Šikola, R. Kekatpure, E. Barnard, J. White, P. Van Dorpe, L. Břínek, O. Tomanec, J. Zlámal, D. Lei, Y. Sonnefraud, *et al.*, Applied physics letters **95**, 253109 (2009).
[6] P. Törmä and W. L. Barnes, Reports on Progress in Physics **78**, 013901 (2014).
[7] S. Campione, J. R. Wendt, G. A. Keeler, and T. S. Luk, Acs Photonics **3**, 293 (2016).
[8] K. O'Brien, H. Suchowski, J. Rho, A. Salandrino, B. Kante, X. Yin, and X. Zhang, Nature Materials **14**, 379 EP (2015).